



Review article

Materials insights into low-temperature performances of lithium-ion batteries



Gaolong Zhu ^a, Kechun Wen ^a, Weiqiang Lv ^a, Xingzhi Zhou ^a, Yachun Liang ^a, Fei Yang ^a, Zhilin Chen ^a, Minda Zou ^a, Jinchao Li ^b, Yuqian Zhang ^a, Weidong He ^{a,*}

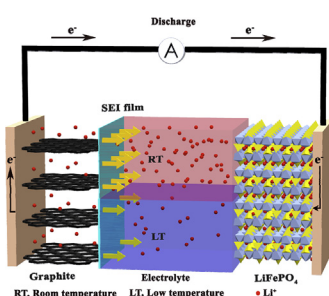
^a School of Energy Science and Engineering, University of Electronic Science and Technology, Chengdu, Sichuan 611731, PR China

^b School of Materials Science and Engineering, Southwest University of Science and Technology, 59 Qinglong Road, Mianyang, Sichuan 621010, PR China

HIGHLIGHTS

- Discusses main limitations of low-temperature performances for lithium batteries.
- Reviews methodology for improving low-temperature lithium batteries.
- Analyzes advanced materials for low-temperature lithium battery performances.

GRAPHICAL ABSTRACT



ARTICLE INFO

Article history:

Received 30 March 2015

Received in revised form

22 August 2015

Accepted 15 September 2015

Available online 22 September 2015

Keywords:

Lithium-ion batteries
Low-temperature performance
Concentration polarization
Electrolyte
Electrode

ABSTRACT

Lithium-ion batteries (LIBs) have been employed in many fields including cell phones, laptop computers, electric vehicles (EVs) and stationary energy storage wells due to their high energy density and pronounced recharge ability. However, energy and power capabilities of LIBs decrease sharply at low operation temperatures. In particular, the charge process becomes extremely sluggish at temperatures below -20°C , which severely limits the applications of LIBs in some cold areas during winter. Extensive research has shown that the electrolyte/electrode composition and microstructure are of fundamental importance to low-temperature performances of LIBs. In this report, we review the recent findings in the role of electrolytes, anodes, and cathodes in the low temperature performances of LIBs. Our overview aims to understand comprehensively the fundamental origin of low-temperature performances of LIBs from a materials perspective and facilitates the development of high-performance lithium-ion battery materials that are operational at a large range of working temperatures.

© 2015 Elsevier B.V. All rights reserved.

1. Introduction

To mitigate the energy crisis and environmental impact of the

fossil-fuel based economy, energy storage technology has been an important component of current energy strategies [1]. Lithium-ion batteries (LIBs) represent a promising energy storage technology for the integration of renewable resources and have been efficient power sources for a large range of applications owing to a number of advantages including high energy density, flexible and lightweight design, and long lifespan [2–8]. Rechargeable LIBs have been available in many commercial applications, such as cell

* Corresponding author. School of Energy Science and Engineering, University of Electronic Science and Technology, Chengdu, Sichuan 611731, PR China.

E-mail address: weidong.he@uestc.edu.cn (W. He).

phones, laptop computers, HEVs, EVs, and stationary energy storage wells. However, the poor low-temperature performances of LIBs limit the applications in cold conditions, such as certain defense and space applications [9,10], and transportation systems, including plug-in hybrid electric vehicles (PHEVs) and electric vehicles (EVs) [11–13]. There is a sharp loss in the energy and power capabilities as the operating temperature is below 0 °C [13–15]. In addition, under –20 °C the lithiation process is typically slower than the delithiation process in the electrode [16]. To avoid the cell damage at low temperatures, the current common method is to increase the working temperature by heating. Nevertheless, this method reduces the energy efficiency, and does not allow for large-scale applications.

In this review, we firstly describe the main existing limitations of LIBs at low temperatures, followed by discussion on the recent improvement in low-temperature performances by developing novel electrolyte, anode and cathode materials. Last, we conclude by providing prospectives on future developments in improving the low-temperature performances of LIBs. This report is focused on elucidating main limitations of low-temperature performances and aims to provide an insightful guidance for enhancing the overall low-temperature performances of LIBs.

2. Main limitations for low-temperature performances of lithium-ion batteries

LIBs lose most energy and capacity as the temperature is below –10 °C [13,14]. Zhang et al. [16] reported that graphite only retains 12% of room temperature capacity at –20 °C. The energy density of 18650 Li-ion batteries decreases from ~100 Wh l^{−1} to ~5 Wh l^{−1}, and the power density decreases from ~800 W l^{−1} to 10 W l^{−1} as the operating temperature decreases from 25 °C to –40 °C [17]. In addition, due to the high charge-transfer resistance at the charged state LIBs can be efficiently charged up only as the temperature is higher than –10 °C [13,18]. Furthermore, the mass transport is hindered at low temperatures due to the increase of inactive lithium ions, giving rise to dendrite formation and growth. This dendritic electrode could lead to battery explosion and damage due to short circuits [19,20]. The poor low-temperature performance hinders substantially further application of LIBs. Here, we discuss the main low-temperature performance limitations of LIBs in the charge/discharge process and structure evolution.

2.1. Main limitations on charge/discharge process

LIBs directly convert chemical energy into electric energy upon discharge. In this process, lithium ions are deintercalated from the layered graphite intercalation host, pass across the solid electrolyte interface (SEI), diffuse through the electrolyte and are intercalated between the LiCoO₂ layers in the cathode [7]. Charge reverses this process and converts electric energy into chemical energy. In the first cycle, a preliminary SEI layer is formed, which has been considered as an essential process for the fabrication of LIBs. The SEI layer protects electrodes and only permits the transport of lithium-ions [21]. The efficient transport of Li⁺ and electrons ensures the efficient operation of LIBs. However, low temperatures impede all the key steps, such as the charge-transfer at electrode/electrolyte interface [22], and Li⁺ transport in the SEI, the electrolyte and the electrodes [13,22,23], leading to the loss in power capability. The commercial electrolyte, LiPF₆ typically dissolves in ethylene carbonate (EC)/ethylmethyl carbonate (EMC) and also freezes at the temperature below –30 °C. Consequently, the slow ionic conduction in such an electrolyte is the major challenge for efficient operation of low-temperature LIBs [9,23]. Wang et al. [24]

also suggested that the resistance of SEI increased by a factor of over 27 at –30 °C and largely limited the low-temperature performance. Huang et al. proposed that the poor performance was caused by the sluggish lithium-ion diffusion in the carbon anode at a low temperature [13]. This indicates that the lithium insertion reaction was kinetically limited at a low temperature. This proposition was then verified by Zhang et al. [15]. The resistance of the batteries is predominated by the charge-transfer resistance R_{ct} as the temperature is below –20 °C. R_{ct} reflects the kinetics of the cell electrochemical reaction. A small R_{ct} value corresponds to a fast kinetics of the electrochemical reaction [15]. In fact, to ensure the operation of the electrolyte at low temperatures, the charge-transfer at the electrode/electrolyte interface must be efficient enough [14,16,25]. Zhang et al. [15] studied the low-temperature performances of LIBs via electrochemical impedance spectroscopy (EIS). Typically, the impedance spectra of LIBs is composed of two overlapping semicircles at high and medium frequency regions, and a straight line at low frequency region. The high and medium frequency regions represent the resistances of SEI (R_{sei}) and electrode/electrolyte interface (R_{ct}), respectively, and the low frequency region represents the Warburg impedance associated with Li⁺ diffusion in the electrode [12,24]. R_b is the bulk resistance of the cell, including the resistances of the electrolyte, separator, and electrodes. Fig. 1 shows that at 3.87 V and 3.45 V, R_{ct} increases substantially at low temperatures [15]. Although R_{sei} and R_b increase with decreasing temperature, the percentage of R_{ct} vs. the total cell resistance achieves nearly 100% as the temperature is below –20 °C. The high charge-transfer resistance at low temperatures results in a high electrochemical polarization [15,17,24,26]. In addition, low-temperature mass transport limitation at the electrode/electrolyte interface increases the deposition of metallic phases on carbon anode, giving rise to concentration polarization [13,14,27,28]. As the deposited lithium is not uniform, the fragile SEI film could be broken under mechanical stress. Continuous deposition of lithium also gives rise to the formation of lithium whiskers that could be easily cut at low temperatures, leading to the accumulation of dendrite [20]. In short, the lithium-ion conductivity is decreased in electrode/electrolyte interface, electrolyte, SEI, anode, and cathode at low temperatures. In all these processes, the low Li⁺ transfer rate at electrode/electrolyte interface caused by low-kinetics electrochemical reaction is the rate-determining step in low-temperature charge and discharge.

The delithiated state has a larger R_{ct} compared with the lithiated state in a Li/graphite cell, and it has been shown that the charge process is slower than the discharge process at –20 °C and –30 °C [16]. In the anode discharge process, lithium-ions leave LiC₆, and C₆ forms [4]. An exothermic electrochemical reaction occurs in this discharge process while the charge experiences an endothermic electrochemical reaction. Lowering the temperature hinders the endothermic electrochemical reaction due to the lack of heat. Thus, lowering the temperature could result in the electrochemical equilibrium moving to lithiated state, making the charge process difficult.

2.2. Main limitation on structure evolution

The structure of materials affects significantly the performance of the batteries. The atomic resolution image in Fig. 2b shows that pristine Li-[Li_{0.2}Ni_{0.2}Mn_{0.6}]O₂ cathode exhibits well-defined layered structure, with a stacking sequence of Li/O/TM (transition metal)/O [29]. Li-[Li_{0.2}Ni_{0.2}Mn_{0.6}]O₂ transforms from layered phase to spinel phase due to the extensive removal of lithium ions during charging (Fig. 2b,c,f). At the same time, part of the lithium ion diffusion channels are blocked by the migration of TM ions to Li layers (Fig. 2f), which leads to capacity degradation. After 300

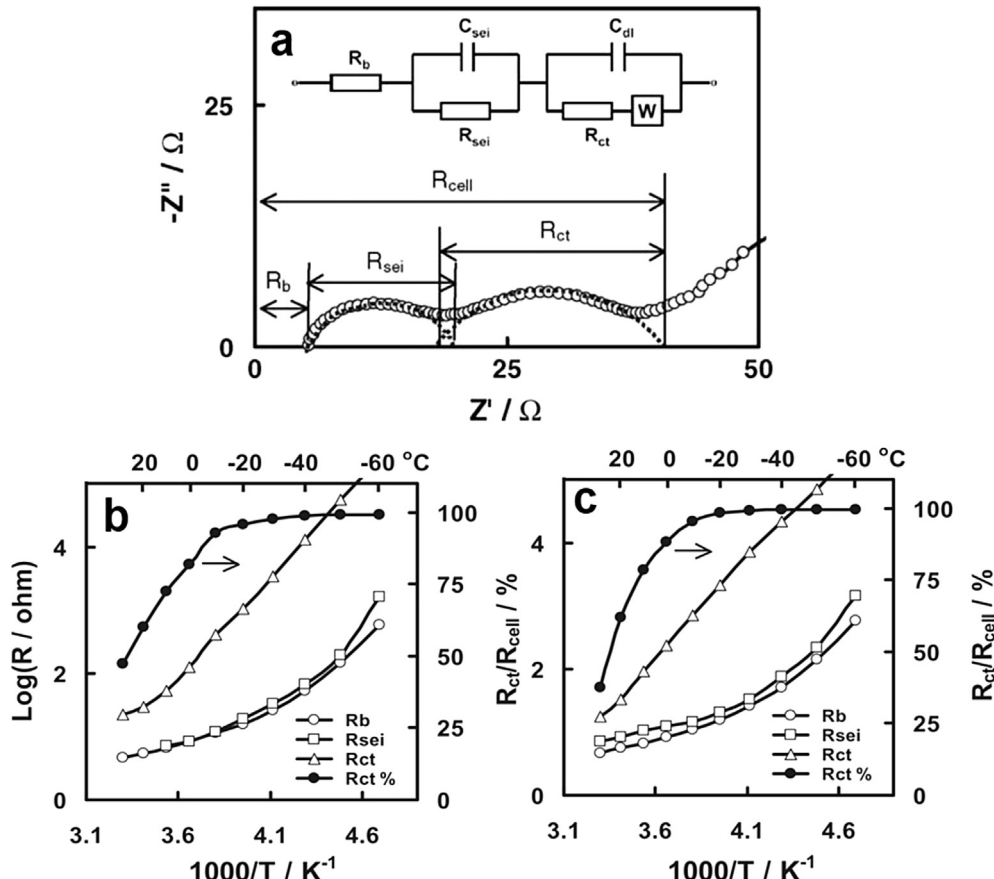


Fig. 1. (a) Typical EISs of the lithium-ion cells and the equivalent circuit used to fit the EIS. Temperature dependences of the R_b , R_{sei} , R_{ct} as well as the R_{ct} percentage. (b) 3.87 V and (c) 3.45 V. (Adopted from Ref. [15].)

cycles, notable microcracks (Fig. 2d) and sponge-like etched surface regions (Fig. 2e,f) are observed clearly in the cycled particles. Some fragment pieces detach from the severely etched surface. Fig. 2g–i shows that the peak drops dramatically at energy loss of ~528 eV in the fragmented pieces compared with the bulk, resulting in the lower valence of Mn ions in the fragmented pieces [29–31]. The gigantic decrease of Mn valence in the fragmented pieces reduces the stored Li species. Wang et al. proposed that the formation of spinel phase and the limited lithium-ions in fragmented pieces dominate the capacity fading during cycling [27,32]. The removal of lithium ions results in the layered structure transforming to spinel phase and blocking lithium ion channels. Low temperatures reduce the lithium-ion transfer rate, which also slows down the phase transition of the layered structure and improves the stability of the cathode. However, there is a giant loss of capacity and voltage at low temperatures, which suggests that the effects of low temperatures on $\text{Li}-[\text{Li}_{0.2}\text{Ni}_{0.2}\text{Mn}_{0.6}]\text{O}_2$ cathode structure are negligible compared with the decrease in the lithium-ion transfer rate at low temperatures.

Low temperatures mainly impede the Li^+ transport in the charge/discharge process. A number of reports have been focused on the low-temperature performance of LIBs. The efforts of improving the low-temperature performance of LIBs mainly focused on decreasing the resistance of lithium-ion transport by improving two aspects: (i) increasing the ionic conductivity of the electrolyte and SEI film [17,23,33–38]; (ii) decreasing the charge-transfer resistance at the electrode/electrolyte interface and lithium ion diffusion resistance in the electrode [23,24,33]. The main practical methods are to improve the electrolyte and develop

advanced electrode materials.

3. Improvement in electrolytes

To improve the low temperature performance, considerable attention has been focused on developing low-temperature electrolytes. The electrolyte solution not only determines the ionic mobility in the electrolyte but also participates in the reaction to form an SEI film on the electrode [21,39]. The SEI film prevents the further electrolyte reduction, protects the electrode, and permits the conduction of lithium ions, which in turn affects the low-temperature performance and cyclic life of LIBs [40]. Low-temperature performance can be achieved successfully, which is attributed to the improvement in the conductivity in electrolytes and the stability of SEI at the electrolyte/electrode interface. On the other hand, experiments have been conducted to optimize the electrolyte system [9,22,23,26,29,31,32,38,41,42], which includes adding suitable cosolvents into the electrolytes and improving the Li salts.

3.1. Improvement in cosolvents

The conductivity of electrolyte solutions drops rapidly at low temperatures due to the relative high freezing points of traditional solvents (EC, DMC) [43]. Much attention has been focused on designing low freezing point but high conductive electrolytes at low temperatures. The main approach is to add suitable cosolvents into electrolytes to reduce the freezing points and the viscosity of the electrolytes. Cosolvents are selected based on several critical

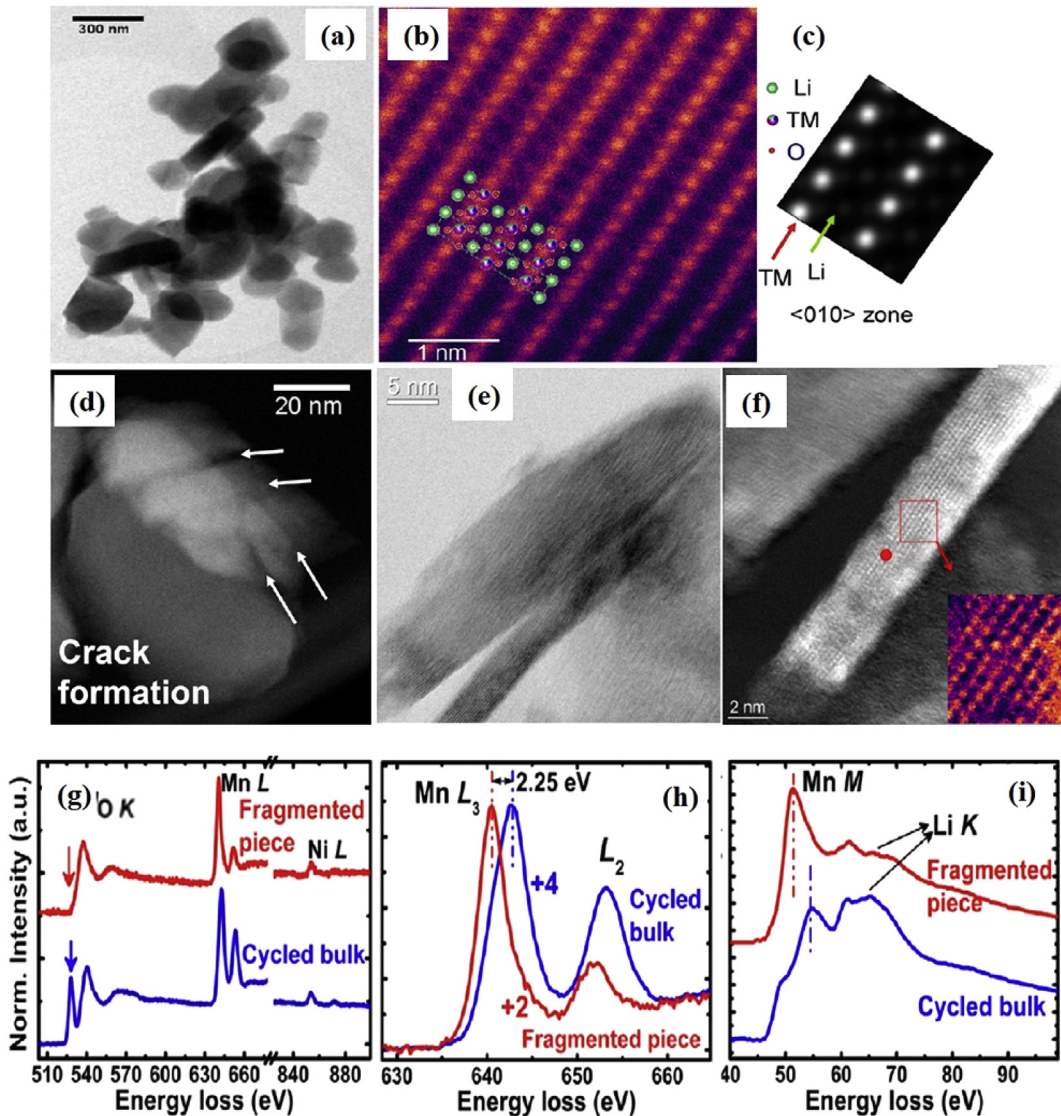


Fig. 2. (a) High-resolution transmission electron microscopy image of the pristine $\text{Li}-\text{Li}_{0.2}\text{Ni}_{0.2}\text{Mn}_{0.6}\text{O}_2$ (LNMO); (b) atomic resolution image; (c) simulated Z-contrast image of the 010 projection with 10% Li/Ni disorder; (d) STEM image showing the formation of microcracks in LNMO after 300 cycles; (e) Bright field image showing lattice fringes the fragmented pieces; (f) Z-contrast image showing the destroyed electrode structure, and the inset shows a magnified view of the region labeled in red rectangle; (g) comparison of O K, Mn L, and Ni L edges; (h) Mn L edge comparison normalized to Mn L₃ peak; (i) Mn M and Li K edge comparison of cycled bulk region and fragmented piece region. (Adopted from Ref. [29].) (For interpretation of the references to colour in this figure legend, the reader is referred to the web version of this article.)

factors, such as high dielectric constant, low viscosity, adequate coordination behavior, wide liquid ranges, and pronounced chemical compatibility [23]. Table 1 shows the physical properties of different cosolvents.

Ein-Eli et al. [36] found that the conductivity values of a binary solvent mixture of methyl formate (MF) and EC containing LiAsF_6 were 25.3 mS/cm and 8.4 mS/cm at 22 °C and –40 °C, respectively. LIBs containing this electrolyte obtained a capacity reversibility of ~50% at –20 °C, which indicates that the addition of MF improves the low temperature performance.

To get further improvement in the conductivity of the electrolyte solution and widen the liquid range of the electrolyte, ternary or quaternary mixtures are used to improve the electrolyte. Compared with single-solvent systems, the multi-components are more tenable and often have a higher conductivity. The disordering effect on lithium ion coordination and physicochemical properties can be readily adjusted through mixed-solvent systems. Smart et al. [23] reported that the lithium-ion cells with the electrolyte of

Table 1
Physical properties of selected aprotic solvents. (Adopted from Ref. [21].)

Solvent	E	H (cp)	Fp (°C)	Bp (°C)
Toluene (tol)	2.379	0.552	–95	111
Ethylmethyl carbonate (EMC)	2.4	0.65	–55	107
Diethyl carbonate (DEC)	2.82	0.748	–43	126
Dimethyl carbonate (DMC)	3.12	0.585	0.5	90
Propyl acetate (PA)	6.00	0.551	–95	102
Ethyl acetate (EA)	6.02	0.426	–84	77
Methyl acetate (MA)	6.67	0.368	–96	56
Methyl formate (MF)	8.90	0.328	–99	36
γ-Butyrolactone (γ-BL)	41.77	1.727	–43	202
Propylene carbonate (PC)	64.92	2.53	–49	241
Ethylene carbonate (EC, 38 °C)	89.6	1.85	36	248

EC–DMC–DEC containing 1 M LiPF_6 exhibit pronounced over 85% capacity retention after 600 cycles at –25 °C. Plichta et al. [9] reported that LIBs with the electrolyte of EC–DMC–EMC containing 1 M LiPF_6 exhibit 52% capacity retention at –40 °C. Huang et al. [13]

revealed that the EC–DEC–DMC–EMC containing 0.8 M LiPF₆ lithium-ion cells have over 60% capacity retention at –30 °C. The lithium-ion cells containing either MF or MA have a high capacity at low temperatures, but the cycle efficiency is low. Shiao et al. [44] reported that cycle efficiency of lithium-ion cells containing MF/MA could be improved by incorporating carbonate solvent or toluene. EC–EMC–MA–tol containing LiPF₆ can cycle ~160 times without significant loss in the capacity and exhibits clearly superior capacity retention at –40 °C. Sazhin et al. [37] reported that EC–DEC–EP and EC–EMC–EP showed promising overall performances at –20 °C, without decay in cyclic life and rate capability. Table 2 lists the formulations of the electrolytes investigated in recent years. Propylene carbonate (PC), ethyl acetate (EA), and methyl butyrate (MB) have been tested as cosolvents for LIB electrolytes. Herreyre et al. [34] revealed that LIBs with EC–DMC–EA/EC–DMC–MB as the electrolyte recovered more than 80% of the initial capacity at –40 °C. Among all the formulations, PC–EC–MB shows the most attractive low-temperature performance. It can retain 98% of the initial capacity at –30 °C. Moreover, this electrolyte exhibits pronounced cyclic capability. The major problem is that the SEI of the PC-based electrolyte is instable, but such a problem has been solved recently by adding methyl vinyl sulfone (MVS) and ethyl vinyl sulfone (EVS) additives [45].

Aliphatic ester cosolvents have shown the capability of improving the low-temperature ionic conductivity of electrolyte solutions. The conductivity decreases with increasing chain length/molecular weight [46]. Meanwhile, electrolytes of a long chain/high-atomic weight molecules show pronounced SEI characteristics [35], which suggests that it can offer adequate kinetics of lithium intercalation. The outstanding properties of SEI facilitates the charge-transfer process of lithium ions and reduces the electrochemical polarization. Accordingly, lithium-graphite cells containing electrolytes of a long chain or higher molecular weight ester cosolvents exhibit improved low-temperature performances, such as propylene carbonate (PC) and methyl butyrate (MB) based electrolytes.

3.2. Improvement in salts

The selection of Li salts affects the lithium ion conductivity and stability of SEI. The optimization of Li salts is important for improving the low-temperature performance. LiPF₆ is a frequently-employed Li salt, but it spontaneously decomposes into LiF and PF₅, which causes structural changes and induces capacity fading. The

replacement of LiPF₆ with lithium tetrafluoroborate (LiBF₄) or lithium bis(oxalato)borate (LiBOB) improves the low-temperature performance since LiBF₄ or LiBOB based electrolytes exhibit lower charge-transfer resistances [41,47–49].

The most significant advantage of LiBOB is its stable SEI on the electrode surface and excellent over-charge tolerance. The major drawbacks are its poor solubility in linear carbonates and relatively high viscosity of solutions, which turns even worse at low temperatures. LiBF₄ based electrolytes show remarkable low-temperature performance for its low charge-transfer resistance at the electrode/electrolyte interface. But the LiBF₄ based electrolyte is relatively inefficient in forming SEI, due to the high capacity loss and the generation of gaseous products in the initial cycle. Lithium oxalyldifluoroborate (LiODFB), which combined the advantages of LiBOB and LiBF₄, was proposed to improve the low-temperature performance [39,50–52]. LiODFB-based electrolytes are advantageous since graphite can be cycled reversibly even with a high concentration (50 wt.%) of propylene carbonate (PC) based electrolyte. This makes it possible to formulate low freezing temperature electrolytes with PC cosolvent and increase the safety of LIBs under overcharge.

The addition of 1–5 mol% LiBOB into LiBF₄–PC based electrolytes facilitates significantly the SEI formation on the surface of graphite [26]. Mandal et al. [43] reported that the mixture of EC–DMC–EMC–PC (15: 37: 38: 10) and 0.9 M LiTFSI was an efficient electrolyte over the temperatures ranged from –30 to 70 °C. Xu et al. [53] designed a thermally stable electrolyte using lactone as solvent and LiBOB/lithium trifluoromethane sulfonate (LiTf) as Li salt, which exhibited stable performances in a wide temperature range from –40 °C to 80 °C with a commercially acceptable performance.

Ionic liquids have been studied extensively as new electrolytes in lithium batteries due to their wide electrochemical windows and pronounced safety features [54,55]. The large-range working temperatures of ionic liquids, from –81 °C to 280 °C [56], have been proposed to be advantageous for improving the low-temperature performances of LIBs. Among the various ionic liquids, those based on anion bis(trifluoromethanesulfonyl)imide (TFSI) have been studied extensively owing to their high stability and pronounced electrochemical performances [57]. Balducci et al. [58] reported that the ionic liquid N-butyl-N-methylpyrrolidininium bis(trifluoromethanesulfonyl) imide (PYR₁₄TFSI) mixed with organic liquid showed a high conductivity of 0.5 mS/cm at –40 °C. Takaya Sato et al. [59] synthesized N,N-diethyl-N-methyl-N-(2-methoxy

Table 2
The performance of lithium-ion cells with various electrolytes.

Formulation	Discharge capacity (compared to room temperature)	Cycling rate	Ref. no.
LiAsF ₆ EC–MF (1:3)	49% (–2 °C)	C/20	[23]
LiPF ₆ EC–DEC (3:7)	67% (–20 °C)	C/20	[23]
LiPF ₆ EC–DMC (3:7)	15% (–20 °C)	C/20	[23]
LiPF ₆ EC–DEC–DMC (1:1:1)	85% (–20 °C)	C/20	[23]
LiPF ₆ EC–DMC–EMC (1:1:1)	52% (–40 °C)	—	[9]
LiPF ₆ EC–EMC–MA–tol (1:1:1)	50% (–40 °C)	C/10	[44]
LiPF ₆ EC–EMC–MA–tol (1:1:1:1)	50% (–40 °C)	C/10	[44]
LiPF ₆ EC–EMC–MA–tol (1:1:1:1)	50% (–40 °C)	C/10	[44]
LiPF ₆ EC–EMC–EP (30:30:40)	87%–89% (–20 °C)	C/5	[37]
LiPF ₆ EC–DEC–EP (30:35:35)	57%–63% (–20 °C)	C/5	[37]
LiPF ₆ EC–DEC–IPA (30:35:35)	72%–75% (–20 °C)	C/5	[37]
LiPF ₆ EC–EMC–EA (30:30:40)	94% (–20 °C)	C/5	[37]
LiPF ₆ EC–DMC–MA (30:30:40)	94% (–20 °C)	C/5	[37]
LiPF ₆ EC–DMC–EA	81% (–40 °C)	C/2	[34]
LiPF ₆ EC–DMC–MB	87% (–40 °C)	C/2	[34]
LiPF ₆ PC–EC–MB	98% (–30 °C)	1C	[34]
LiPF ₆ PC–EC–EMC (1:1:3)	83% (–30 °C)	—	[22]

ethyl)ammonium bis(trifluoromethylsulfonyl) imide (DEME-TFSI) and achieved a high conductivity of 0.8 mS/cm at 0 °C. Makoto et al. [60] fabricated a double-layer capacitor with ionic liquid 1-ethyl-3-methylimidazolium fluoride (EMIF) 2.3 HF as electrolyte, which exhibited a high conductivity of 30 mS/cm at –30 °C. Despite the complexity of the route to certain ionic liquid electrolytes, the advances in the field facilitate the development of low-temperature LIBs.

4. Improvement in electrodes

Lithium-ion batteries have been proposed as power sources of EVs or HEVs [61]. The basic requirements for EVs or HEVs are high energy densities. However, the limited lithium diffusion in the electrodes and the high charge-transfer resistance at high charging–discharging rates cause a high polarization, and lead to limited low-temperature performances [62].

The kinetic limitation of the lithium-ion transfer at the electrode/electrolyte interface results in the main disadvantage of the low-temperature performances. The improvement of the low-temperature performance is concentrated on optimizing the electrochemical reaction (faradic reaction) by reducing R_{ct} and keeping the SEI stability. Accordingly, there have been various methods for improving anode performance such as mild oxidation, coating, mixing, and developing novel anode materials [63]. On the other hand, the improvement in cathode is also studied extensively, including decreasing the particle size, coating, constructing 3D structure materials, and developing novel cathode materials [12]. However, anodes and cathodes consist of different materials and their low temperature properties are substantially different. In addition, the characteristics of SEI depend much on electrode and electrolyte materials. Next, we will discuss the improvement in the anodes, cathodes, and their SEI properties.

4.1. Improvement in anode

Graphite is the most common anode material for LIBs. The major drawback is its dissatisfied low-temperature performances [13,16,17], which has been attributed to the high R_{ct} at the electrolyte–electrode interface, the instability of SEI and reduced solid-state lithium diffusivity. We then discuss the effective methodology for the improvement in such anodes.

4.1.1. Mild oxidation

Mild oxidation of graphite leads to a reduction of unsaturated carbon atoms at the edge planes, smaller mean particle size as well as formation of nanovoids, nanochannels, and chemically bonded SEI [64]. These result in a decrease in the electrochemical impedance, hindering the co-intercalation of solvated lithium-ions and the decomposition of electrolyte. Consequently, the low-temperature performance is improved after the mild oxidation. Mild oxidation of graphite can be easily achieved by thermal treatment or wet chemical oxidation [65–67].

4.1.2. Mixing

Mildly-oxidized graphite mixed with metal nanoparticles has shown improvement in low-temperature performances. The oxidized graphite electrodes mixed with 1% Cu and Sn in a 1 M LiPF₆ EC–DEC–DMC (1:1:1) electrolyte have capacities of 130 mAh g^{−1} [64] and 94 mAh g^{−1} at –30 °C, respectively [68]. The outstanding low-temperature performance has been attributed to the enhancement of lithium-ions desolvation, the increase of SEI conductivity and the internal conductivity of the bulk electrode of metal-dispersed powders [68].

4.1.3. Coating

The oxidized graphite electrodes coated with 50 Å Cu and Sn layers in a 1 M LiPF₆ EC–DEC–DMC (1:1:1) electrolyte have the capacity of 103 mAh g^{−1} [65] and 152 mAh g^{−1} [68] at –30 °C, respectively. Gao et al. [69] prepared a Cu-coated graphitic carbon anode by a plating method. The attractive stable SEI suppresses the decomposition of the electrolyte (1 M LiClO₄ PC–DMC, 1:1 by volume) and suggests the promising application of the LIBs at –60 °C [69]. Therefore, the existence of metal layers on the anode leads to a remarkable decrease in R_{ct} , a stable SEI, and an increased lithium conductivity [68–70].

Ag–Fe₂O₃/carbon nanofibers (CNFs) anode materials exhibit pronounced electrochemical performances at a low temperature (–5 °C) due to its synergistic effects of the CNF matrix and the conducting Ag [71]. Then, Li et al. developed Fe/Fe₃C–CNF materials, which delivered a high capacity of 250 mAh g^{−1} after 55 cycles at –5 °C in a 1 M LiPF₆ EC–EMC–DMC (1:1:1 in volume) electrolyte [72].

4.1.4. Novel anode materials

Recently, Raccichini et al. [73] synthesized multilayer graphene anode materials through combination of microwave irradiation and ultra-sonication in an ionic liquid. The comparison between the low temperature performances of multilayer crystalline graphene (GRAL) and commercial graphite SLP30 in 1 M LiClO₄ PC–DMC (1:1 by volume) electrolyte is shown in Fig. 3. It shows that the capacity of GRAL is higher than SLP30 at low temperatures. The outstanding low-temperature performance has been attributed to its high active surface area. The high surface area results in high efficiency of anodic electrochemical reaction, enhancing the kinetics of lithium-ion diffusion.

Li₄Ti₅O₁₂ is another promising low-temperature anode due to its outstanding cycling stability. However, the sluggish lithium-ion and electron conductivity results in a poor electrochemical performance. Reducing particle size of Li₄Ti₅O₁₂ and coating are two common ways to improve the electrochemical performance [74,75]. Fig. 4 shows the discharge profiles of the Li₄Ti₅O₁₂ and Li₄Ti₅O₁₂/C anodes at various temperatures. The carbon-coated Li₄Ti₅O₁₂ anode materials are promising for low-temperature applications [76]. The conductivity of Li₄Ti₅O₁₂ anode increased ~3 orders after coating. The effects of particle size on the low-temperature performance are dependent on the charging/discharging rates [77]. Marinaro et al. [78] prepared nanosized rutile TiO₂ via a sol–gel method, which delivered a capacity of 77 mAh g^{−1} at –40 °C at a C/5 rate in a 1 M LiClO₄ PC–DMC (1:1 by volume) electrolyte.

4.2. Improvement in cathode

Surface modification on lithium cobalt oxides (LiCoO₂), lithium nickel oxides (LiNiO₂), and spinel-type lithium manganese oxides (LiMn₂O₄) has been the main approach to improve cathodes [63]. Here we mainly discuss the improvement in lithium iron phosphate (LiFePO₄) and a few novel low-temperature cathodes.

LiFePO₄ is considered as a promising cathode of LIBs for HEVs, EVs and stationary energy storage in China and the US [79]. It has attracted extensive interests due to its appealing advantages, such as intrinsic thermal stability, low cost, non-toxicity, safety, and environmental benignity [80–83]. However, the insulating nature and sluggish kinetics of both electron and lithium-ion transport seriously limit its low-temperature performances and charge/discharge rates [79,84,85]. The conductivity of the pristine compound is ~10^{−9} S cm^{−1} [86] and the Li⁺ diffusivity is ~10^{−14}–10^{−16} cm² S^{−1} [87], which severely limits its electrochemical response [88]. LiFePO₄ has an ordered-olivine structure with a space group of *Pnma*. The 1D diffusion channel of Li⁺ is easily

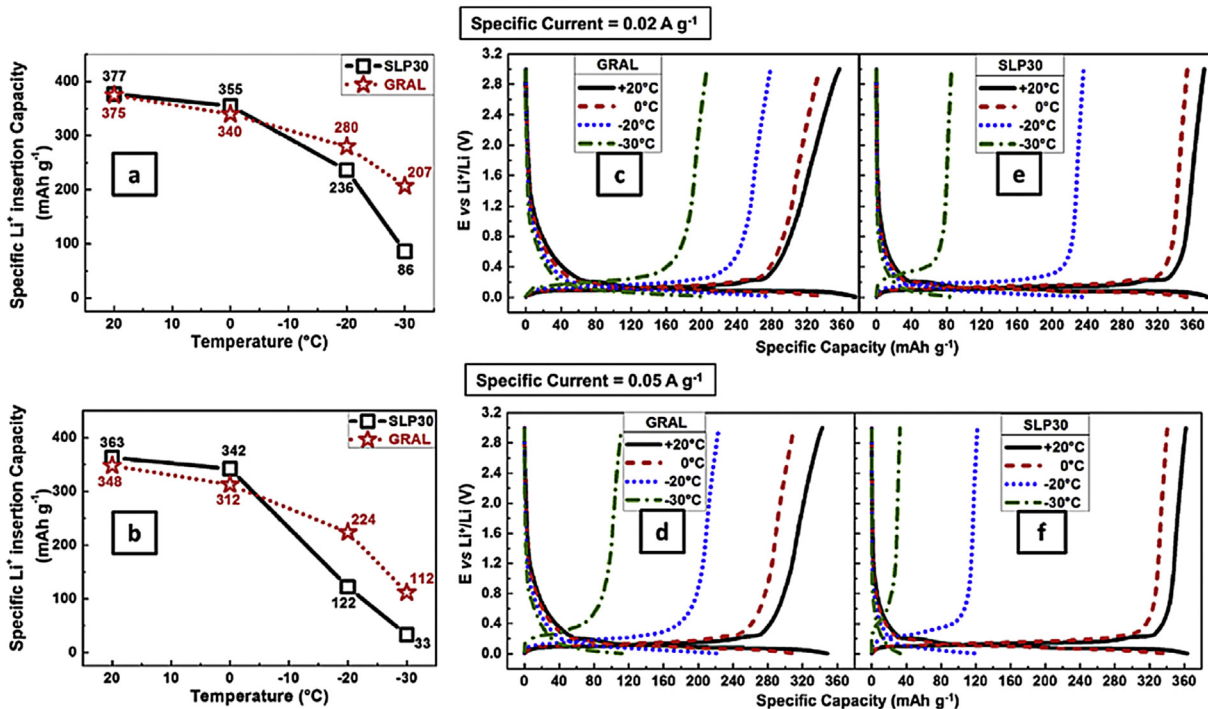


Fig. 3. Comparison between the low temperature performances of multilayer crystalline graphene (GRAL) and commercial graphite SLP30 at two different currents (0.02 A g^{-1} and 0.05 A g^{-1}). (a, b) Capacity evolution between 20°C and -30°C . Influence of the temperature on the voltage profiles of GRAL (c, d), and graphite (e, f). Electrolyte: 1 M LiPF_6 in EC:DEC:DMC 1:1:1 (w/w). (Adopted from Ref. [73].)

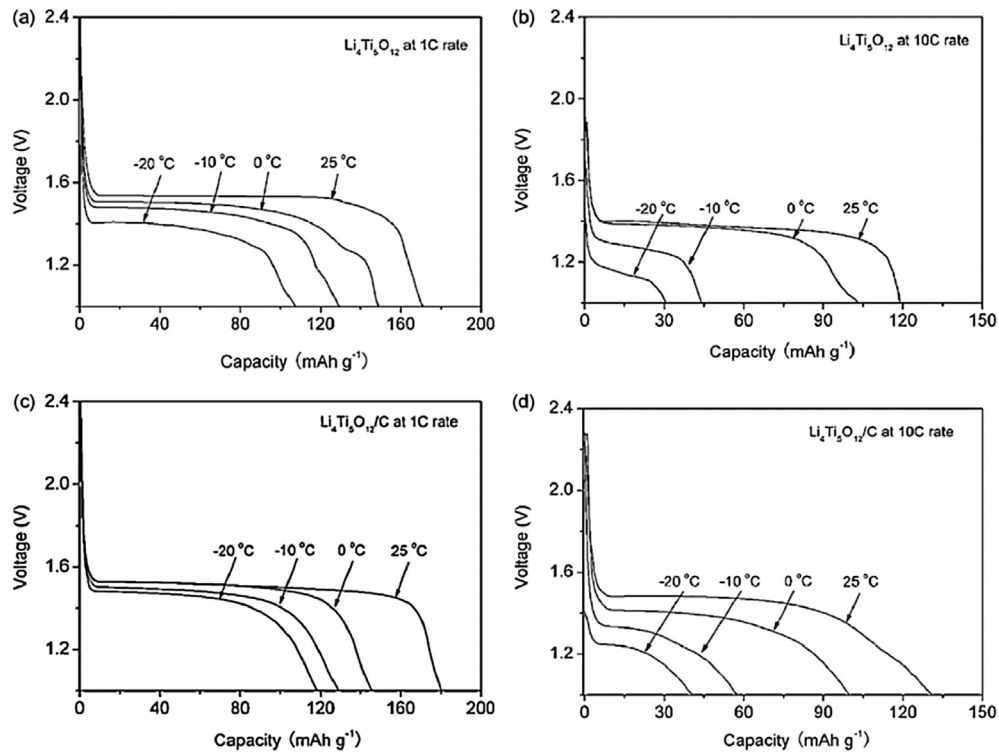


Fig. 4. The discharge profiles of the $\text{Li}_4\text{Ti}_5\text{O}_{12}$ anodes (a) at a 1C rate; (b) at a 10C rate at various temperatures and $\text{Li}_4\text{Ti}_5\text{O}_{12}/\text{C}$ anodes (c) at a 1C rate; (d) at a 10C rate at various temperatures. (Adopted from Ref. [76].)

blocked by impurities or defects, resulting in lower diffusivity and reduced availability of active volume [89].

Much attention has been focused on improving lithium ion

diffusion, SEI stability, and electronic conductivity of LiFePO_4 cathodes at low temperatures. The methodology includes decreasing the particle size of LiFePO_4 [62,90], coating

electronically conductive materials [91–96], and constructing three-dimensional conducting networks [97,98].

4.2.1. Decreasing particle size

Decreasing particle size can provide shorter diffusion path length for lithium ions and electrons, a larger electrolyte/electrode surface area for Li^+ insertion and extraction, thus, leading to the improvement in the electrochemical kinetics and low-temperature performances [99,100]. Sides et al. [100] proposed that the specific capacity in a 1 M LiClO_4 EC–DEC–DMC (1:1:1) electrolyte with a V_2O_5 nanofiber cathode is two orders of magnitude greater compared with microfiber at low temperatures. However, nanoparticles can lead to more side reactions due to high surface area and reactivity [7]. In addition, a large amount of binders are needed to glue these small particles together, which inevitably decreases the capacity [101]. Decreasing particle size has also been applied to other cathode materials such as LiCoO_2 , LiMn_2O_4 , and V_2O_5 for the improvement of low-temperature performances [7,62].

To avoid problems associated with nanoparticle electrodes, such as reactive surfaces and poor particle contact, and also retain the advantages of the nanostructures, extensive attention has been focused on efforts including coating conductive materials and forming nanostructured electrodes.

4.2.2. Coating

Similar to the carbon anode, there still exist electrolyte decomposition layers (EDL) on cathode surfaces [102]. The electrochemical behavior on cathode surfaces strongly depends on the properties of EDL [19,103]. The components of electrolyte decomposition layers on cathode are temperature sensitive [104] and are dependent of the types of electrolyte materials [103]. The common components for all cathodes are LiF , ROCO_2M , ROLi , MCO_3 , ROCO_2Li , Li_2CO_3 , MF_2 (M = transition metal), polycarbonates [19]. In particular, the EDL formed on LiFePO_4 cathode are different from Li_xMO_y host materials (M = Ni, Mn) due to its pronounced stability [105]. In general, the thickness of EDL on LiFePO_4 is less than 5 nm in a 1 M LiPF_6 mixture of EC and DEC. LiFePO_4 cathode coated with a carbonaceous material could avoid the undesirable reactions and improve the stability of EDL [98,106–114]. This coating method significantly prevents the contamination from HF, water, etc [19]. Compared with the pristine LiFePO_4 , the capacity retention of a carbon coating LiFePO_4 is increased from 53.4% to 66.1% at -25°C [12]. The appropriate thin carbon coating is necessary to ensure the balance of sufficient conductivity and easy lithium-ion penetration [115]; high electronic conductivity carbon such as graphite is extremely desirable [116,117]. Uniform and full carbon coating is required for LiFePO_4 particles to host electrons from all directions and ensure a low polarization [79]. The decomposition/pyrolysis of organic carbon sources can form a more uniform graphitic carbon film [118]. Increasing the surface area of the porous carbon film enhances the conductivity [119]. Excessive carbon decreases the tap density of LiFePO_4 seriously and leads to the generation of by-products such as Fe_2P [111,120], whose effect on the electrochemical performance is still in debate [25]. Hence, an efficient carbon content in LiFePO_4/C is less than 5 wt.% [3]. Wang et al. [91] developed a low cost method to prepare nano-sized LiFePO_4/C cathodes. The discharge capacity of the synthetic composite in a 1 M LiClO_4 EC–DMC (1:1 by volume) electrolyte is 168 mAh g⁻¹ at 0.6C and 90 mAh g⁻¹ at 60C. Oh et al. [93] reported a synthetic route to double carbon coating over LiFePO_4 , as shown in Fig. 5. The formation procedures for spherical nano-porous LiFePO_4 include four steps: the formation of $\text{FePO}_4 \cdot \text{H}_2\text{O}$, carbon coated nano-sized FePO_4 , lithium impregnation, and carbon networking with porosity. At -20°C in the LiPF_6 EC–DEC electrolyte, the 1 C capacity retention of this double carbon coating LiFePO_4 can achieve ~50% of

that at 25°C .

Attaching conductive polymers, such as polypyrrole (PPy) and polyaniline (PANI) to LiFePO_4/C particles, is another efficient and cost-effective way to improve the low-temperature performance of LiFePO_4 . Chen et al. [96] showed that the polymer PANI film coating in the pore space between carbon-coated LiFePO_4 (C-LFP) particles reduced the charge-transfer impedance. Xie et al. designed a spherical LFP structure coated by a specific π -bond character planar polymer and displayed a high capacity at low temperatures [121]. Huang et al. adopted electrochemical deposition [122] and simultaneous chemical polymerization [123] to prepare LFP/PPy and LFP/PANI composite cathodes. These cathodes showed excellent conductivity of lithium ions and electrons, and the specific capacity reached almost the theoretical value at a low rate and retained more than 70% at a high rate of 20C. Conductive polymers were also proposed as a binder with a reduced cathode weight. This type of composite cathodes exhibited a high energy density as well as a high power density.

4.2.3. Three-dimensional conducting network

For further improvement in the conductivity and the electrochemical properties, three-dimensional conducting network is required. Kim et al. prepared an excellent cathode material without any additional conductive agent. The as-prepared LiFePO_4 -nanographite platelet (NGP) heterostructure improves electron transport [108]. Wu et al. [12] designed and prepared three-dimensional nano-carbon decorated LiFePO_4 nanocomposites, which exhibited an ultrahigh rate capability and a superior low temperature performance. Fig. 6 shows the crystal structure, topographical characterization, and prepared schematic illustration of the $\text{LiFePO}_4/\text{C}/\text{CNT}$ nanocomposite. The capacity retentions and middle discharge voltages of pristine LiFePO_4 , single-wall decorated LiFePO_4/C , and single-wall nanotubes $\text{LiFePO}_4/\text{CNTs}$ at temperatures in the range of -25°C to 25°C are shown in Fig. 7. The designed $\text{LiFePO}_4/\text{C}/\text{CNTs}$ exhibited excellent low-temperature performance and electrochemical properties. The capacity retention in a 1 M LiPF_6 EC–DMC–DEC (1:1:1, in wt%) electrolyte was ~71.4% upon discharging at -25°C compared with that at 25°C . These properties may be resulted from the synergistic effect of the amorphous uniform carbon coating on all LiFePO_4 nanoparticles and the decreased internal resistance by the graphitized conductive CNTs forming a three-dimensional conducting network in the entire electrode. Kim et al. [124] developed a catalyst assisted self-assembly method to embed graphene onto LiFePO_4 as a cathode material, which showed excellent cycling performance and rate-capability.

4.2.4. Novel cathode materials

Much research has focused on $\text{Li}[\text{Ni}_x\text{Co}_y\text{Mn}_{1-x-y}]O_2$ (NMC) materials due to their high rate performance, capacity, and the structure stability [125]. The low-temperature performances of NMC electrodes have been rarely reported. Yoon et al. investigated the low-temperature performance of NMC cathodes with a 1.2 M EC–EMC (3:7 by volume) electrolyte [126]. Fig. 8 shows the initial discharge curves, discharge capacity, and cycle lives of $\text{Li}[\text{Li}|\text{Ni}_x\text{Co}_y\text{Mn}_{1-x-y}]O_2$ powders ($x = 1/3, 0.5, 0.6, 0.7, 0.8$, and 0.85) at various temperatures. The results show that the low-temperature capacity of NMC cathodes is dependent on their chemical composition and increases with increase Ni composition. Since a high Ni composition leads to a high electric conductivity, $\text{Li}[\text{Ni}_{0.85}\text{C}_{0.075}\text{Mn}_{0.075}]O_2$ delivers a capacity of 127 mAh g⁻¹ at -20°C . Smart et al. reported $\text{Li}_{1+x}(\text{Co}_{1/3}\text{Ni}_{1/3}\text{Mn}_{1/3})_{1-x}O_2$ cathodes in 1.2 M EC–EMC (20:80) electrolyte showed ~55% capacity retention at -40°C at a high discharge rate [127]. The authors suggested that the low ethylene carbonate content was beneficial for realizing a

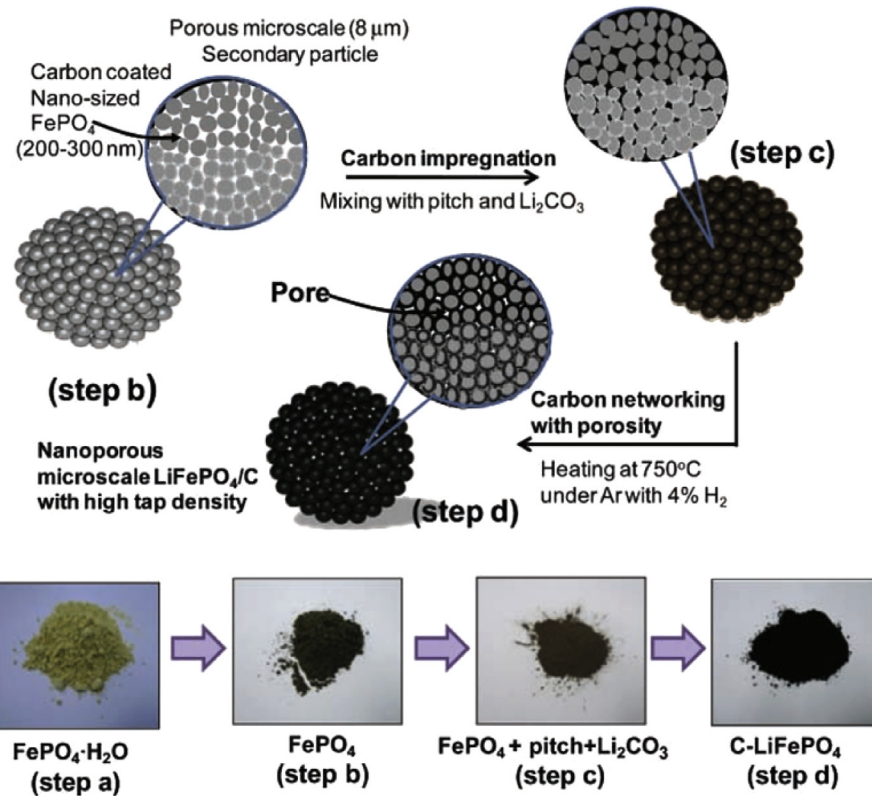


Fig. 5. Schematic of formation procedure for spherical microscale nano-porous LiFePO_4 and photographs of materials formed during the four steps. (Adopted from Ref. [93].)

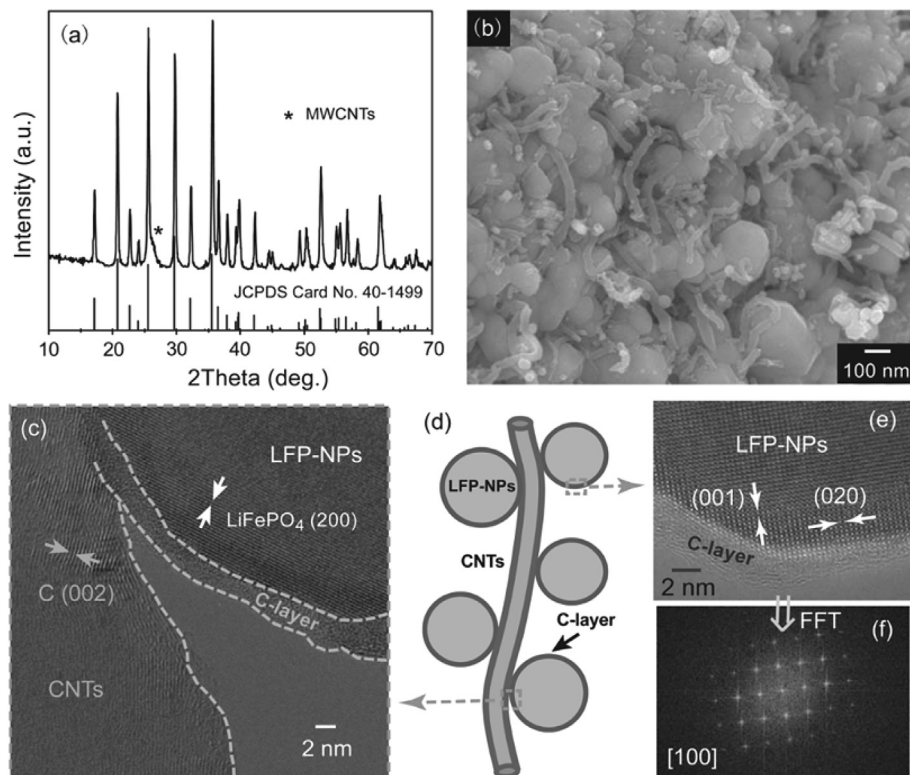


Fig. 6. (a) XRD pattern, (b) SEM, (c, e) HRTEM images, (d) schematic illustration of the prepared $\text{LiFePO}_4@\text{C}/\text{CNT}$ nanocomposite, and (f) corresponding FFT of the HRTEM in (e). (Adopted from Ref. [12].)

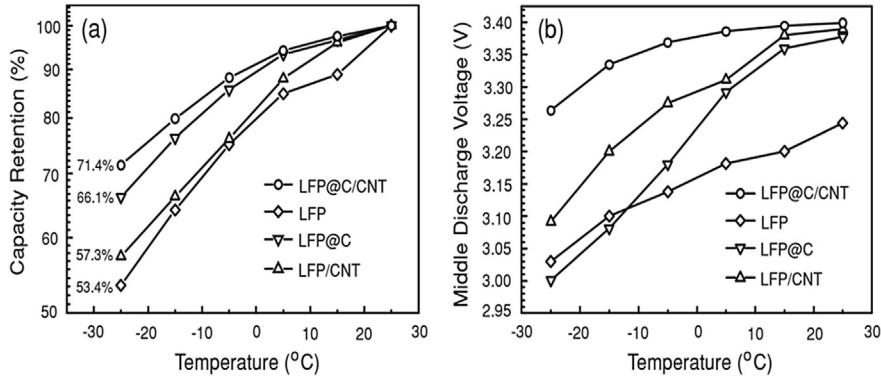


Fig. 7. The dependences of (a) capacity retention and (b) middle discharge voltage on temperature in the range of $-25\text{ }^{\circ}\text{C}$ to $25\text{ }^{\circ}\text{C}$ for $\text{LiFePO}_4@\text{C/CNT}$, $\text{LiFePO}_4@\text{C}$, $\text{LiFePO}_4/\text{CNT}$, and pristine LiFePO_4 . All the samples were tested in the voltage range of 2.2 V – 2.4 V vs. Li^+/Li at the same discharge rate of 0.2 C . (Adopted from Ref. [12].)

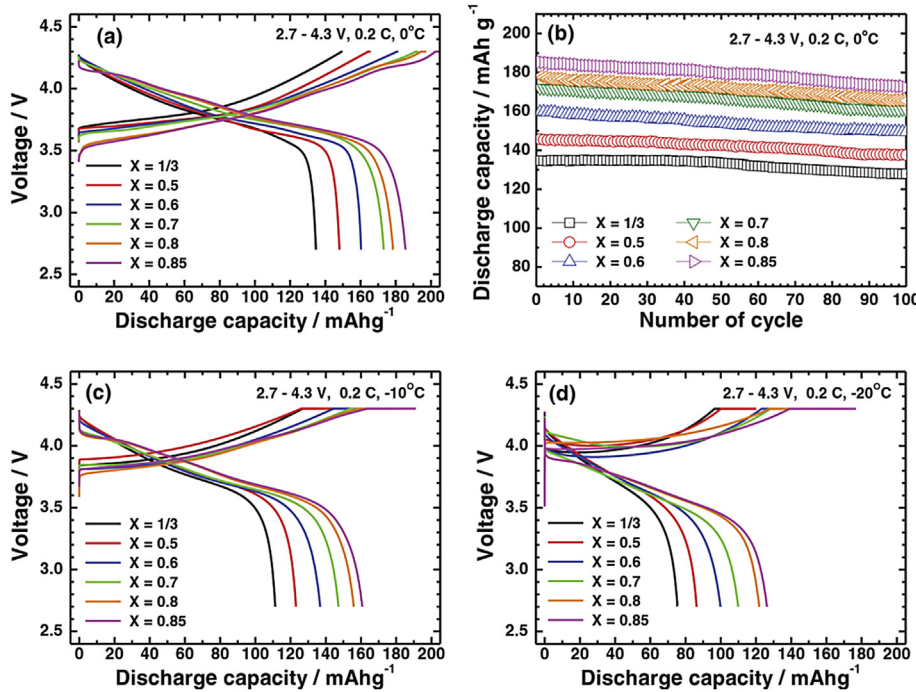


Fig. 8. (a) Initial discharge curves of $\text{Li}/[\text{Li}_{\text{x}}\text{Co}_{\text{y}}\text{Mn}_{1-\text{x}-\text{y}}]\text{O}_2$ powders ($\text{x} = 1/3, 0.5, 0.6, 0.7, 0.8$, and 0.85) at $0\text{ }^{\circ}\text{C}$. (b) Cycle lives of $\text{Li}/[\text{Li}_{\text{x}}\text{Co}_{\text{y}}\text{Mn}_{1-\text{x}-\text{y}}]\text{O}_2$ powders ($\text{x} = 1/3, 0.5, 0.6, 0.7, 0.8$, and 0.85) at $0\text{ }^{\circ}\text{C}$. (c) Discharge capacity of $\text{Li}/[\text{Li}_{\text{x}}\text{Co}_{\text{y}}\text{Mn}_{1-\text{x}-\text{y}}]\text{O}_2$ powders ($\text{x} = 1/3, 0.5, 0.6, 0.7, 0.8$, and 0.85) at $-10\text{ }^{\circ}\text{C}$ and (d) at $-20\text{ }^{\circ}\text{C}$. The applied current density across the positive electrode was 40 mAh g^{-1} (0.2 C) in the voltage range of 2.7 – 4.3 V . (Adopted from Ref. [126].)

high discharge rate owing to a lower viscosity and a higher ionic conductivity. On the other hand, the low-temperature cycling stability of $\text{Li}(\text{Ni}_{0.8}\text{Co}_{0.15}\text{Al}_{0.05})\text{O}_2$ was remarkably enhanced by AlF_3 coating [128].

Rui et al. reported that $\text{Li}_3\text{V}_2(\text{PO}_4)_3/\text{C}$ (LVP/C) delivered a high discharge capacity of 108.1 mAh g^{-1} at $-20\text{ }^{\circ}\text{C}$. The promising low-temperature performance was attributed to a lower activation energy of LVP, as calculated to be 6.57 kJ mol^{-1} . It suggests the easier extraction/intercalation of lithium ions in LVP [129].

5. Prospectives

Although the low-temperature performances of cathodes have been improved with various methods, their applications at low temperature conditions are still limited. Since the operation of LIBs is based on multiple components involving electrolytes, anodes

and cathodes, efforts of improving the low-temperature performances of all the materials are required to achieve promising overall low-temperature properties. We propose several research topics for improving the low-temperature performance of LIBs. First, the correlation between lithium-ion transfer at the interface and temperature decrease should be quantitatively investigated under various conditions [130]. Second, the properties of SEI films directly affect the low temperature performances, and the formation mechanism of SEI films and the associated effect of temperatures are subject to further study. Third, further studies should be focused on developing facile routes to ionic liquid electrolytes with solid low-temperature properties. Then, the size and morphology of battery materials, such as LiFePO_4 , are challenging to manipulate in actual synthesis, and the effects of particle size, morphology and structure of the electrodes on low temperature performances of LIBs should also be explored further [131–133].

6. Conclusion

The performance of LIBs undergoes severe degradation at low temperatures. The low temperature impedes all the key steps in the operation of LIBs and the increased electrochemical polarization results in poor low-temperature performances. The key point is to provide expedite paths for the transport of Li^+ and electrons at low temperatures. Managing the electrolyte and developing electrodes are efficient methods to improve the low-temperature performance. Further studies should be focused on realizing more applicable performance of cost-effective and durable LIBs that are expected to be highly-efficient in a large range of working temperatures.

Acknowledgments

The work is supported by UESTC new faculty startup fund, the National Natural Science Foundation (grant no. 21403031) and the Fundamental Research Funds for the Chinese Central Universities (grant no. ZYGX2014J088).

References

- [1] K.B. Hueso, M. Armand, T. Rojo, *Energy Environ. Sci.* 6 (2013) 734–749.
- [2] J. Garcia-Barriocanal, A. Rivera-Calzada, M. Varela, Z. Sefrioui, E. Iborra, C. Leon, S.J. Pennycook, J. Santamaría, *Science* 321 (2008) 676–680.
- [3] L.X. Yuan, Z.H. Wang, W.X. Zhang, X.L. Hu, J.T. Chen, Y.H. Huang, J.B. Goodenough, *Energy Environ. Sci.* 4 (2011) 269–284.
- [4] M. Armand, J.M. Tarascon, *Nature* 451 (2008) 652–657.
- [5] B. Kang, G. Ceder, *Nature* 458 (2009) 190–193.
- [6] N.S. Choi, Z. Chen, S.A. Freunberger, X. Ji, Y.K. Sun, K. Amine, G. Yushin, L.F. Nazar, J. Cho, P.G. Bruce, *Angew. Chem. Int. Ed.* 51 (2012) 9994–10024.
- [7] P.G. Bruce, B. Scrosati, J.M. Tarascon, *Angew. Chem. Int. Ed.* 47 (2008) 2930–2946.
- [8] W. He, B. Wang, *Adv. Energy Mater.* 2 (2012) 329–333.
- [9] E.J. Plichta, W.K. Behl, *J. Power Sources* 88 (2000) 192–196.
- [10] E.J. Plichta, M. Hendrickson, R. Thompson, G. Au, W.K. Behl, M.C. Smart, B.V. Ratnakumar, S. Surampudi, *J. Power Sources* 94 (2001) 160–162.
- [11] W. Chang, S.J. Kim, I.T. Park, B.W. Cho, K.Y. Chung, H.C. Shin, *J. Alloys Compd.* 563 (2013) 249–253.
- [12] X.L. Wu, Y.G. Guo, J. Su, J.W. Xiong, Y.L. Zhang, L.J. Wan, *Adv. Energy Mater.* 3 (2013) 1155–1160.
- [13] C.K. Huang, J.S. Sakamoto, J. Wolfenstein, S. Surampudi, *J. Electrochem. Soc.* 147 (2000) 2893–2896.
- [14] H. Lin, D. Chua, M. Salomon, H.C. Shiao, M. Hendrickson, E. Plichta, S. Slane, *Electrochem. Solid State Lett.* 4 (2001) A71–A73.
- [15] S.S. Zhang, K. Xu, T.R. Jow, *Electrochim. Acta* 49 (2004) 1057–1061.
- [16] S.S. Zhang, K. Xu, T.R. Jow, *Electrochim. Acta* 48 (2002) 241–246.
- [17] G. Nagasubramanian, *J. Appl. Electrochem.* 31 (2001) 99–104.
- [18] S.S. Zhang, K. Xu, J.L. Allen, T.R. Jow, *J. Power Sources* 110 (2002) 216–221.
- [19] D. Aurbach, E. Zinigrad, Y. Cohen, H. Teller, *Solid State Ionics* 148 (2002) 405–416.
- [20] J.-i. Yamaki, S.-i. Tobishima, K. Hayashi, K. Saito, Y. Nemoto, M. Arakawa, *J. Power Sources* 74 (1998) 219–227.
- [21] S. Zhang, K. Xu, T. Jow, *Electrochim. Acta* 51 (2006) 1636–1640.
- [22] X.-Z. Liao, Z.-F. Ma, Q. Gong, Y.-S. He, L. Pei, L.-J. Zeng, *Electrochim. Commun.* 10 (2008) 691–694.
- [23] M. Smart, B. Ratnakumar, S. Surampudi, *J. Electrochem. Soc.* 146 (1999) 486–492.
- [24] W. Chunsheng, A.J. Appleby, F.E. Little, *J. Electrochem. Soc.* 149 (2002) A754–A760.
- [25] S.Y. Chung, J.T. Bloking, Y.M. Chiang, *Nat. Mater.* 1 (2002) 123–128.
- [26] S.S. Zhang, K. Xu, T.R. Jow, *J. Power Sources* 156 (2006) 629–633.
- [27] M. Ma, J. Tu, Y. Yuan, X. Wang, K. Li, F. Mao, Z. Zeng, *J. Power Sources* 179 (2008) 395–400.
- [28] K. Xu, *Chem. Rev.* 104 (2004) 4303–4418.
- [29] J. Zheng, M. Gu, J. Xiao, P. Zuo, C. Wang, J.G. Zhang, *Nano Lett.* 13 (2013) 3824–3830.
- [30] B. Xu, C.R. Fell, M. Chi, Y.S. Meng, *Energy Environ. Sci.* 4 (2011) 2223–2233.
- [31] M. Gu, A. Genc, I. Belharouak, D. Wang, K. Amine, S. Thevuthasan, D.R. Baer, J.-G. Zhang, N.D. Browning, J. Liu, *Chem. Mater.* 25 (2013) 2319–2326.
- [32] A. Ito, K. Shoda, Y. Sato, M. Hatano, H. Horie, Y. Ohsawa, *J. Power Sources* 196 (2011) 4785–4790.
- [33] S. Zhang, K. Xu, T. Jow, *J. Power Sources* 115 (2003) 137–140.
- [34] S. Herreyre, O. Huchet, S. Barusseau, F. Perton, J.M. Bodet, T. Biensan, *J. Power Sources* 97–98 (2001) 576–580.
- [35] M.C. Smart, B.V. Ratnakumar, S. Surampudi, *J. Electrochem. Soc.* 149 (2002) A361–A370.
- [36] Y. Ein-Eli, S.R. Thomas, R. Chadha, T.J. Blakley, V.R. Koch, *J. Electrochem. Soc.* 144 (1997) 823–829.
- [37] S.V. Sazhin, M.Y. Khimchenko, Y.N. Tritenichenko, H.S. Lim, *J. Power Sources* 87 (2000) 112–117.
- [38] E. Plichta, M. Hendrickson, R. Thompson, G. Au, W. Behl, M. Smart, B. Ratnakumar, S. Surampudi, *J. Power Sources* 94 (2001) 160–162.
- [39] S.S. Zhang, *J. Power Sources* 163 (2007) 713–718.
- [40] B.V. Ratnakumar, M.C. Smart, S. Surampudi, *J. Power Sources* 97–98 (2001) 137–139.
- [41] S.S. Zhang, K. Xu, T.R. Jow, *Electrochim. Commun.* 4 (2002) 928–932.
- [42] M.C. Smart, B.V. Ratnakumar, L. Whitcanack, S. Surampudi, J. Byers, R. Marsh, *IEEE Aerosp. Electron. Syst. Mag.* 14 (1999) 36–42.
- [43] B.K. Mandal, A.K. Padhi, Z. Shi, S. Chakraborty, R. Filler, *J. Power Sources* 162 (2006) 690–695.
- [44] H.C. Shiao, D. Chua, H.P. Lin, S. Slane, M. Salomon, *J. Power Sources* 87 (2000) 167–173.
- [45] R. Wagner, S. Brox, J. Kasnatscheew, D.R. Gallus, M. Amereller, I. Cekic-Laskovic, M. Winter, *Electrochim. Commun.* 40 (2014) 80–83.
- [46] S.S. Zhang, *J. Power Sources* 162 (2006) 1379–1394.
- [47] T.R. Jow, M.S. Ding, K. Xu, S.S. Zhang, J.L. Allen, K. Amine, G.L. Henriksen, *J. Power Sources* 119–121 (2003) 343–348.
- [48] X. Kang, S.S. Zhang, L. Unchul, J.L. Allen, T.R. Jow, *J. Power Sources* 146 (2005) 79–85.
- [49] D. Abraham, J. Heaton, S.H. Kang, D. Dees, A. Jansen, *J. Electrochem. Soc.* 155 (2008) A41–A47.
- [50] S. Shui Zhang, *Electrochim. Commun.* 8 (2006) 1423–1428.
- [51] H.Q. Gao, Z.A. Zhang, Y.Q. Lai, J. Li, Y.X. Liu, *J. Central South Univ. Technol.* 15 (2008) 830–834.
- [52] H.M. Zhou, F.R. Liu, J. Li, *Appl. Mech. Mater.* 152 (2012) 1106–1111.
- [53] K. Xu, S. Zhang, T.R. Jow, *Electrolyte Formulations for Wide Temperature Lithium Ion Batteries*, 2014, Google Patents.
- [54] M. Armand, F. Endres, D.R. MacFarlane, H. Ohno, B. Scrosati, *Nat. Mater.* 8 (2009) 621–629.
- [55] L. Lombardo, S. Brutti, M.A. Navarra, S. Panero, P. Reale, *J. Power Sources* 227 (2013) 8–14.
- [56] M. Galinski, A. Lewandowski, I. Stępiński, *Electrochim. Acta* 51 (2006) 5567–5580.
- [57] G.B. Appetecchi, M. Montanisno, D. Zane, M. Carewska, F. Alessandrini, S. Passerini, *Electrochim. Acta* 54 (2009) 1325–1332.
- [58] R.-S. Kühnel, N. Böckenfeld, S. Passerini, M. Winter, A. Balducci, *Electrochim. Acta* 56 (2011) 4092–4099.
- [59] T. Sato, T. Maruo, S. Marukane, K. Takagi, *J. Power Sources* 138 (2004) 253–261.
- [60] M. Ue, M. Takeda, A. Toriumi, A. Kominato, R. Hagiwara, Y. Ito, *J. Electrochem. Soc.* 150 (2003) A499–A502.
- [61] J.-M. Tarascon, M. Armand, *Nature* 414 (2001) 359–367.
- [62] Y. Wang, G. Cao, *Adv. Mater.* 20 (2008) 2251–2269.
- [63] L. Fu, H. Liu, C. Li, Y. Wu, E. Rahm, R. Holze, H. Wu, *Solid State Sci.* 8 (2006) 113–128.
- [64] F. Nobili, S. Dsoke, T. Mecozzi, R. Marassi, *Electrochim. Acta* 51 (2005) 536–544.
- [65] M. Mancini, F. Nobili, S. Dsoke, F. D'Amico, R. Tossici, F. Croce, R. Marassi, *J. Power Sources* 190 (2009) 141–148.
- [66] X. Cao, J.H. Kim, S.M. Oh, *Electrochim. Acta* 47 (2002) 4085–4089.
- [67] Y. Wu, C. Jiang, C. Wan, R. Holze, H. Wu, *J. Power Sources* 111 (2002) 329–334.
- [68] F. Nobili, M. Mancini, S. Dsoke, R. Tossici, R. Marassi, *J. Power Sources* 195 (2010) 7090–7097.
- [69] J. Gao, L. Fu, H. Zhang, T. Zhang, Y. Wu, H. Wu, *Electrochim. Commun.* 8 (2006) 1726–1730.
- [70] G. Wang, J. Gao, L. Fu, N. Zhao, Y. Wu, T. Takamura, *J. Power Sources* 174 (2007) 1109–1112.
- [71] M. Zou, J. Li, W. Wen, L. Chen, L. Guan, H. Lai, Z. Huang, *J. Power Sources* 270 (2014) 468–474.
- [72] J. Li, W. Wen, G. Xu, M. Zou, Z. Huang, L. Guan, *Electrochim. Acta* 153 (2015) 300–305.
- [73] R. Raccichini, A. Varzi, V.S.K. Chakravadhanula, C. Kübel, A. Balducci, S. Passerini, *J. Power Sources* 281 (2015) 318–325.
- [74] T. Yuan, R. Cai, K. Wang, R. Ran, S. Liu, Z. Shao, *Ceram. Int.* 35 (2009) 1757–1768.
- [75] Z. Wen, X. Yang, S. Huang, *J. Power Sources* 174 (2007) 1041–1045.
- [76] T. Yuan, X. Yu, R. Cai, Y. Zhou, Z. Shao, *J. Power Sources* 195 (2010) 4997–5004.
- [77] J. Allen, T. Jow, J. Wolfenstein, *J. Power Sources* 159 (2006) 1340–1345.
- [78] D. Aurbach, *J. Power Sources* 89 (2000) 206–218.
- [79] O.K. Park, Y. Cho, S. Lee, H.C. Yoo, H.-K. Song, J. Cho, *Energy Environ. Sci.* 4 (2011) 1621–1633.
- [80] A.K. Padhi, K. Nanjundaswamy, J.B.d. Goodenough, *J. Electrochem. Soc.* 144 (1997) 1188–1194.
- [81] B. Ellis, W. Makahoun, Y. Makimura, K. Toghill, L. Nazar, *Nat. Mater.* 6 (2007) 749–753.
- [82] Y. Wang, Y. Wang, E. Hosono, K. Wang, H. Zhou, *Angew. Chem.* 120 (2008) 7571–7575.
- [83] Y. Wu, Z. Wen, J. Li, *Adv. Mater.* 23 (2011) 1126–1129.
- [84] M. Contestabile, G. Offer, R. Slade, F. Jaeger, M. Thoennes, *Energy Environ. Sci.* 4 (2011) 3754–3772.

- [85] S.W. Kim, D.H. Seo, H. Kim, K.Y. Park, K. Kang, *Phys. Chem. Chem. Phys.* 14 (2012) 3299–3303.
- [86] S.Y. Chung, Y.-M. Chiang, *Electrochem. Solid State Lett.* 6 (2003) A278–A281.
- [87] P.P. Prosini, M. Lisi, D. Zane, M. Pasquali, *Solid State Ionics* 148 (2002) 45–51.
- [88] P.S. Herle, B. Ellis, N. Coombs, L. Nazar, *Nat. Mater.* 3 (2004) 147–152.
- [89] D. Morgan, A. Van der Ven, G. Ceder, *Electrochem. Solid State Lett.* 7 (2004) A30–A32.
- [90] R. Dedryvere, M. Maccario, L. Croguennec, F. Le Cras, C. Delmas, D. Gonbeau, *Chem. Mater.* 20 (2008) 7164–7170.
- [91] Y. Wang, Y. Wang, E. Hosono, K. Wang, H. Zhou, *Angew. Chem.* 120 (2008) 7571–7575.
- [92] C. Zhu, Y. Yu, L. Gu, K. Weichert, J. Maier, *Angew. Chem. Int. Ed.* 50 (2011) 6278–6282.
- [93] S.W. Oh, S.T. Myung, S.M. Oh, K.H. Oh, K. Amine, B. Scrosati, Y.K. Sun, *Adv. Mater.* 22 (2010) 4842–4845.
- [94] D. Lepage, C. Michot, G. Liang, M. Gauthier, S.B. Schougaard, *Angew. Chem. Int. Ed.* 50 (2011) 6884–6887.
- [95] C. Sun, S. Rajasekharan, J.B. Goodenough, F. Zhou, *J. Am. Chem. Soc.* 133 (2011) 2132–2135.
- [96] W.M. Chen, Y.H. Huang, L.X. Yuan, *J. Electroanal. Chem.* 660 (2011) 108–113.
- [97] X.L. Wu, L.Y. Jiang, F.F. Cao, Y.G. Guo, L.J. Wan, *Adv. Mater.* 21 (2009) 2710–2714.
- [98] H. Ji, L. Zhang, M.T. Pettes, H. Li, S. Chen, L. Shi, R. Piner, R.S. Ruoff, *Nano Lett.* 12 (2012) 2446–2451.
- [99] A.S. Aricò, P. Bruce, B. Scrosati, J.M. Tarascon, W. Van Schalkwijk, *Nat. Mater.* 4 (2005) 366–377.
- [100] C.R. Sides, C.R. Martin, *Adv. Mater.* 17 (2005) 125–128.
- [101] L.H. Hu, F.Y. Wu, C.T. Lin, A.N. Khlobystov, L.J. Li, *Nat. Commun.* 4 (2013) 1687.
- [102] K. Edström, T. Gustafsson, J.O. Thomas, *Electrochim. Acta* 50 (2004) 397–403.
- [103] A. Churikov, *Electrochim. Acta* 46 (2001) 2415–2426.
- [104] M. Marinaro, M. Pfanzelt, P. Kubiak, R. Marassi, M. Wohlfahrt-Mehrens, *J. Power Sources* 196 (2011) 9825–9829.
- [105] A. Andersson, A. Henningson, H. Siegbahn, U. Jansson, K. Edström, *J. Power Sources* 119 (2003) 522–527.
- [106] L. Wang, H. Wang, Z. Liu, C. Xiao, S. Dong, P. Han, Z. Zhang, X. Zhang, C. Bi, G. Cui, *Solid State Ionics* 181 (2010) 1685–1689.
- [107] N. Ravet, Y. Chouinard, J. Magnan, S. Besner, M. Gauthier, M. Armand, *J. Power Sources* 97 (2001) 503–507.
- [108] Y.C. Chang, C.T. Peng, I.M. Hung, *J. Mater. Sci.* 49 (2014) 6907–6916.
- [109] H. Kim, H. Kim, S.W. Kim, K.Y. Park, J. Kim, S. Jeon, K. Kang, *Carbon* 50 (2012) 1966–1971.
- [110] T. Zhu, B. Xia, L. Zhou, X.W.D. Lou, *J. Mater. Chem.* 22 (2012) 7851–7855.
- [111] H.X. Ji, X.L. Wu, L.Z. Fan, C. Krien, I. Fiering, Y.G. Guo, Y. Mei, O.G. Schmidt, *Adv. Mater.* 22 (2010) 4591–4595.
- [112] C. Julien, A. Mauger, A. Ait-Salah, M. Massot, F. Gendron, K. Zaghib, *Ionics* 13 (2007) 395–411.
- [113] A.A. Salah, A. Mauger, C. Julien, F. Gendron, *Mater. Sci. Eng. B* 129 (2006) 232–244.
- [114] D. Aurbach, B. Markovsky, G. Salitra, E. Markevich, Y. Talyossef, M. Koltypin, L. Nazar, B. Ellis, D. Kovacheva, *J. Power Sources* 165 (2007) 491–499.
- [115] Z.R. Chang, H.J. Lv, H.W. Tang, H.J. Li, X.Z. Yuan, H. Wang, *Electrochim. Acta* (2009) 4595–4599.
- [116] Y. Hu, M.M. Doeff, R. Kostecki, R. Finones, *J. Electrochem. Soc.* 151 (2004) A1279–A1285.
- [117] M.M. Doeff, J.D. Wilcox, R. Kostecki, G. Lau, *J. Power Sources* 163 (2006) 180–184.
- [118] Y.H. Nien, J.R. Carey, J.S. Chen, *J. Power Sources* 193 (2009) 822–827.
- [119] X.L. Wu, L.Y. Jiang, F.F. Cao, Y.G. Guo, L.J. Wan, *Adv. Mater.* 21 (2009) 2710–2714.
- [120] B. Ellis, P.S. Herle, Y.H. Rho, L. Nazar, R. Dunlap, L.K. Perry, D. Ryan, *Faraday Discuss.* 134 (2007) 119–141.
- [121] H.M. Xie, R.S. Wang, J.R. Ying, L.Y. Zhang, A.F. Jalbout, H.Y. Yu, G.L. Yang, X.M. Pan, Z.M. Su, *Adv. Mater.* 18 (2006) 2609–2613.
- [122] Y.-H. Huang, K.S. Park, J.B. Goodenough, *J. Electrochem. Soc.* 153 (2006) A2282–A2286.
- [123] Y.-H. Huang, J.B. Goodenough, *Chem. Mater.* 20 (2008) 7237–7241.
- [124] W. Kim, W. Ryu, D. Han, S. Lim, J. Eom, H. Kwon, *ACS Appl. Mater. Interfaces* 6 (2014) 4731–4736.
- [125] S.J. Yoon, K.J. Park, B.B. Lim, C.S. Yoon, Y.K. Sun, *J. Electrochem. Soc.* 162 (2015) A3059–A3063.
- [126] S.J. Yoon, S.T. Myung, Y.K. Sun, *J. Electrochem. Soc.* 161 (2014) A1514–A1520.
- [127] M. Smart, J. Whitacre, B. Ratnakumar, K. Amine, *J. Power Sources* 168 (2007) 501–508.
- [128] B.C. Park, H.B. Kim, H.J. Bang, J. Prakash, Y.K. Sun, *Ind. Eng. Chem. Res.* 47 (2008) 3876–3882.
- [129] X. Rui, Y. Jin, X. Feng, L. Zhang, C. Chen, *J. Power Sources* 196 (2011) 2109–2114.
- [130] A.V. Virkar, *J. Power Sources* 196 (2011) 5970–5984.
- [131] Y. Liang, K. Wen, Y. Mao, Z. Liu, G. Zhu, F. Yang, W. He, *ChemElectroChem* 2 (2015).
- [132] J. Liu, M.N. Banis, Q. Sun, A. Lushington, R. Li, T.K. Sham, X. Sun, *Adv. Mater.* 26 (2014) 6472–6477.
- [133] Y. Liang, K. Wen, Y. Mao, Z. Liu, G. Zhu, F. Yang, W. He, *ChemElectroChem* 2 (2015) 1227–1237.